Oxygen vacancy and hydrogen in amorphous HfO_2

Benoît Sklénard, Lukas Cvitkovich, Dominic Waldhoer, Jing Li

▶ **To cite this version:**

Benoît Sklénard, Lukas Cvitkovich, Dominic Waldhoer, Jing Li. Oxygen vacancy and hydrogen in amorphous HfO_2. Journal of Physics D: Applied Physics, 2023, 56 (24), pp.245301. 10.1088/1361-6463/acc878 . cea-04194022

HAL Id: cea-04194022
https://cea.hal.science/cea-04194022v1

Submitted on 1 Sep 2023

HAL is a multi-disciplinary open access archive for the deposit and dissemination of scientific research documents, whether they are published or not. The documents may come from teaching and research institutions in France or abroad, or from public or private research centers.

L'archive ouverte pluridisciplinaire **HAL**, est destinée au dépôt et à la diffusion de documents scientifiques de niveau recherche, publiés ou non, émanant des établissements d'enseignement et de recherche français ou étrangers, des laboratoires publics ou privés.

Oxygen Vacancy and Hydrogen in Amorphous HfO_2

Benoît Sklénard,[1,2] Lukas Cvitkovich,[3] Dominic Waldhoer,[3] and Jing Li[1,2,*]

[1] *Université Grenoble Alpes, CEA, Leti, F-38000, Grenoble, France*
[2] *European Theoretical Spectroscopy Facility (ETSF), F-38000 Grenoble*
[3] *Institute for Microelectronics, Technische Universität Wien*

Amorphous hafnium dioxide (a-HfO_2) is widely used in electronic devices, such as ultra-scaled field-effect transistors and resistive memory cells. The density of oxygen vacancy (OV) defects in a-HfO_2 strongly influences the conductivity of the amorphous material. Ultimately, OV defects are responsible for the formation and rupture of conductive filament paths which are exploited in novel resistive switching devices. In this work, we studied neutral OV in a-HfO_2 using *ab initio* methods. We investigated the formation energy of OV, the binding energy of di-OVs, the OV migration, unperturbed and in the close presence of a hydrogen atom, as well as the migration of hydrogen atom towards OV. A shallow and short-range OV migration barrier (0.6 eV) exists in a-HfO_2 in contrast to the barrier (2.4 eV) in crystalline HfO_2. Nearby hydrogen has a limited impact on the OV migration; however, hydrogen can diffuse easily by hopping among OVs.

I. INTRODUCTION

Amorphous hafnium dioxide (a-HfO_2) is the material of choice for electronic devices, with many promising applications in computer-component microelectronics and non-volatile memory. For example, it serves as a dielectric material in complementary metal-oxide-semiconductor technology due to its high dielectric constant [1–3], also playing the essential part in resistive memory devices that store information by forming/breaking conducting filaments[3–6]. The oxygen vacancy (OV) in a-HfO_2 has the principal contribution to the leakage current in transistors [7]. It is also responsible for formation of conductive filaments in memristors[8, 9]. OVs are dominant defects in thin HfO_2 layer on silicon [1, 10–13], especially considering low-temperature processes required for novel 3D integration techniques, which generally lead to larger defect concentrations compared to processes with a higher thermal budget [14]. Moreover, hydrogen is introduced during the material growth process for the passivation of dangling bonds [15, 16].

Although a-HfO_2 is used in devices, most of the theoretical studies are based on crystalline HfO_2, especially monoclinic HfO_2 (m-HfO_2). Capron *et al.* investigated OV migration in m-HfO_2 along different reaction paths, demonstrating that the energy barrier of neutral OV migration is about 2 eV [17]. Duncan *et al.* reported that hydrogen can stabilize OV in m-HfO_2 [16]. Bradley *et al.* examined the binding energy of adjacent OVs in m-HfO_2, which is about 0.15 eV, indicating the tendency of OV clustering [18]. Strand *et al.* simulated the creation of OV and interstitial oxygen under an electric field, pointing out the importance of extra electrons for this process to occur [19]. These studies based on crystalline material served as a first step to the understanding of OV and hydrogen in HfO_2, but the simulation of a-HfO_2 is inevitable. The main challenge to simulating a-HfO_2 is its amorphous nature, which requires larger system sizes and statistical treatment in order to provide representative results. Despite these challenges, a few studies based on a-HfO_2 have been carried out. Kaviani *et al.* investigated the interaction of hydrogen atoms in a-HfO_2 [20]. Gao *et al.* reported that the formation energy of the second OV is lower than the first OV by 0.1 eV on average, but with a large standard deviation (0.4 eV) in a-HfO_2 [21].

In this work, we performed a systematic investigation of OVs and their interactions with atomic hydrogen in a-HfO_2. The starting point was to study the OV formation energy, proceeding with di-OVs binding energy, and finally considering migrating OVs, unperturbed or affected by the nearby hydrogen atoms.

II. METHODS

The OV defect-free a-HfO_2 model is obtained by melting and quenching a cubic 3x3x3 HfO_2 supercell using a classical force field of the Pedone type with parameters from previous work [22]. First, the temperature is increased up to 7400 K, well above the melting point of HfO_2. Then, the structure is relaxed for 10 ps at 8000 K and quenched with a cooling rate of 17.75 K/ps. The resulting amorphous model consists of 108 hafnium and 216 oxygen atoms in a cubic unit cell with an edge length of 16.45 Å. The atomic structure of the a-HfO_2 model is further optimized using density functional theory (DFT) (Fig. 1a). An OV defect is created by removing an oxygen atom in the unit cell, followed by the structural relaxation at the DFT level (Fig. 1b). An OV results in a defect state in the bandgap, which localizes an additional electron around the OV, as shown in Fig. 1c. The same method is applied to generate structures with di-OVs. The hydrogen-oxygen (HO) defect is generated by substituting an oxygen atom with a hydrogen atom, followed by structural relaxation. For structural relaxation, the convergence threshold was set at 10^{-5} eV for the total energy. DFT calculations were performed us-

* Jing.Li@cea.fr

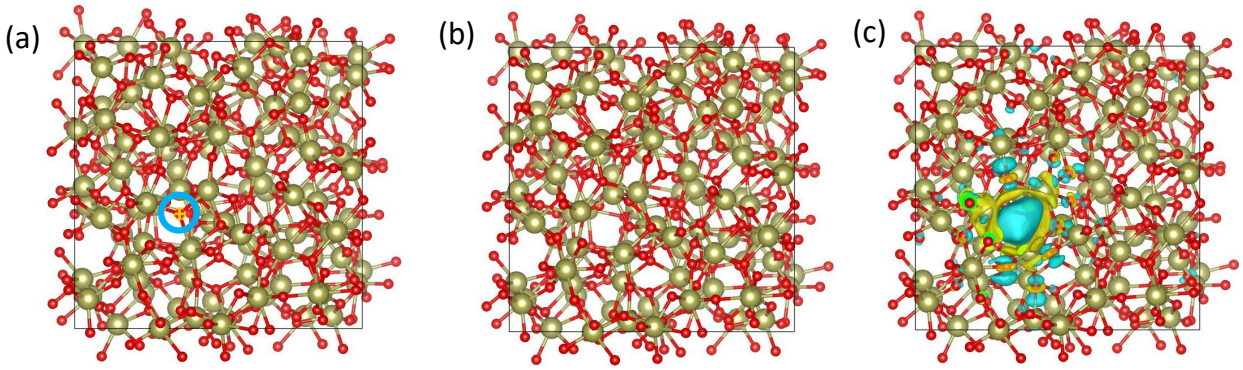

FIG. 1. (a) The structure of the a-HfO_2 model, which was used in this study. A cubic unit cell with edge length 16.45 Å contains 108 hafnium and 216 oxygen atoms. (b) An example of a structure with an OV by removing an oxygen atom indicated by the blue circle in (a) and followed by a structural relaxation. (c) The charge density of an additional electron, which is localized on the OV. The additional electron density is the difference between the charge density in cation and neutral DFT calculations.

ing VASP [23] with the PBE functional [24]. Due to the large cell used, we restricted the Brillouin zone sampling to the gamma point. The cut-off energy for the plane-wave basis-set is set at 400 eV, and total energy in the self-consistent electron density calculation is converged within 10^{-8} eV. Energy barriers for OV and HO migration are computed using the climbing-image nudged elastic band (NEB) method [25, 26] implemented in Transition State Tools for VASP.

III. RESULTS

A. Formation energy of single OV

From the bond length distributions of the a-HfO_2 model shown in Fig. 2a, the O-Hf bond has a sharp peak centered approximately at 2.1 Å. In contrast, the O-O and Hf-Hf bond lengths feature wide bands corresponding to the positions of the first nearest neighbors. By counting the neighboring Hf atoms with distance cut-off 2.7 Å[27], the coordination number of oxygen is determined. As shown in Fig. 2b, the majority (167 out of 216) of OVs are with the coordination number of 3. For corrdinations number 2 and 4, there are 26 and 23 OVs. By using Bader charge analysis [28], we noticed that the excess charge of oxygen atoms increases for higher coordination numbers, as shown in Fig. 2c; while OV atomic volume displays the inverse dependence (Fig. 2d).

The formation energy (E_f) of single neutral OV is calculated as:

$$E_f = E_{OV} - (E_0 - \mu_O), \tag{1}$$

where E_{OV} and E_0 are the total energies with and without OV, and μ_O is the chemical potential of an oxygen atom, taken from the half of ground state energy for an oxygen molecule (O_2). We calculated formation energies for all possible OVs in our model, 216 in total. The median energies obtained for oxygen coordination numbers 2, 3 and 4 (Fig. 3a) are 6.33, 6.27, and 6.00 eV, respectively. Hence, over-coordinated oxygen atoms favor the formation of vacancies. If the oxygen coordination number is not taken into account, the median formation energy value of 6.17 eV is obtained for the entire ensemble of OVs, which is in accordance with previous studies [18, 29] that reported values of 6.5 eV for a-HfO_2 and 6.75 eV for m-HfO_2. However, the distribution of E_f (Fig. 3b) is asymmetric, showing a tail towards the smaller energy. This fact can be attributed to the amorphous nature of the structure, producing multiple peaks in the O-O bond length distribution (Fig. 2a). Therefore, a vacancy can be formed with less effort if an oxygen atom is removed from a site located close to another oxygen atom due to repulsive interaction between them. Figure 3c confirms that the lowest formation energies are obtained for the sites corresponding to smaller distances between the oxygen atoms. It suggests that these sites might be the "weak spots" in a-HfO_2, which can form the very first few OVs, facilitating the creation of conductive filament in a resistive memory device, or conducting leakage current in the high-k oxide in a transistor.

B. Binding energy of di-OVs

The tendency of OV clustering is indicated by the binding energy. The binding energy of neutral di-OVs can be read from the formation energies of di-OVs and individual OVs. However, the term for the energy of a single oxygen atom in Eq. 1 cancels out, yielding the final formula:

$$E_b = E_f(OVi) + E_f(OVj) - E_f(OVi, OVj) \tag{2}$$
$$= (E_{OVi} + E_{OVj}) - (E_{OVi,OVj} + E_{bulk}), \tag{3}$$

where $E_{OVi,OVj}$ is the total energy for a structure containing two OVs. In order to evaluate the binding ener-

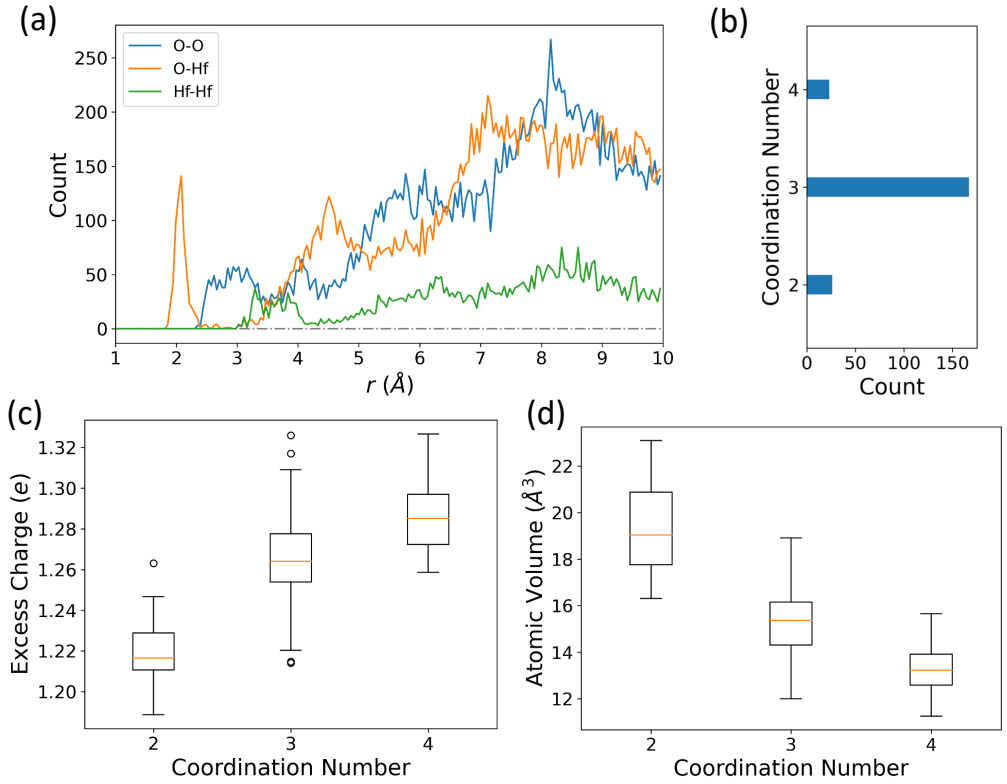

FIG. 2. Principal characteristics of the OVs: (a) Bond length distribution in the a-HfO_2 model; (b) Occurrence of OVs with different oxygen coordination numbers: 2 - 26 occurrences, 3 - 167 occurrences, and 4 - 23 occurrences; in total, 216 cases were considered; (c) Excess charge; (d) OV volume as a function of oxygen coordination number, calculated by employing the Bader charge analysis.

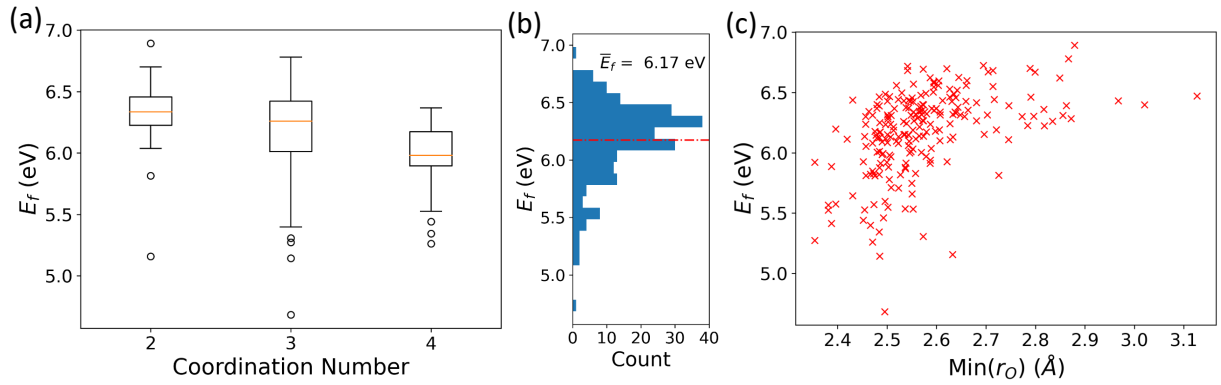

FIG. 3. (a) Formation energy of a single neutral OV as a function of oxygen coordination number. The median energy values are 6.33, 6.27, and 6.00 eV for coordination numbers 2, 3, and 4, respectively; (b) Formation energy distribution of 216 OVs featuring the median value of 6.17 eV; (c) OV formation energy as a function of the distance between the oxygen atoms.

gies for di-OVs, we picked one particular OV with coordination number 3 and formation energy of 6.35 eV (its position is shown in Fig. 1a) and removed the second oxygen from one of the remaining 215 possible sites. Fig. 4a shows the binding energy versus the distance between the two OVs, and Fig. 4b displays the same data re-plotted as box-and-whisker plot with 2 Åbins. The binding energy does not depend much on the distance. The averaged binding energy is slightly below zero at −0.08 eV and the median is at −0.05 eV. Negative binding energy implies averagely repulsive interaction between OVs. However, such a weak interaction together with the broad distribution of binding energies ranging from negative to positive values (as shown in Fig. 4b and Fig. 4d, see also

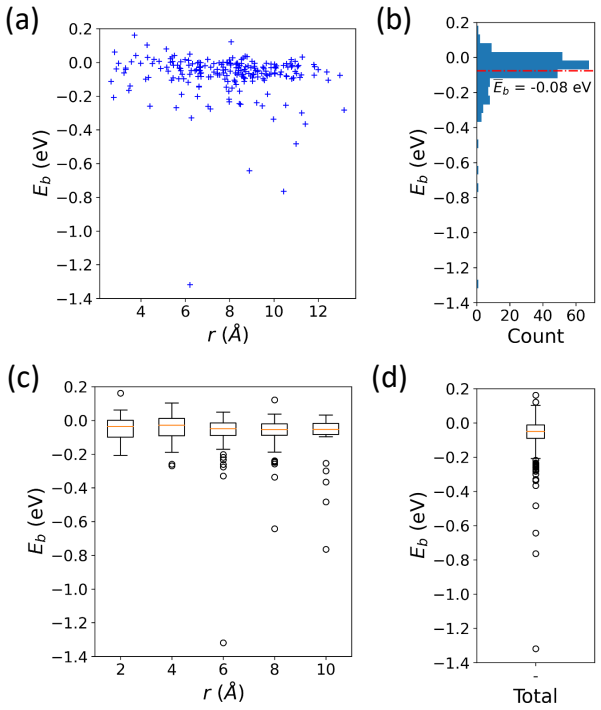

FIG. 4. Scatter (a) and box-and-whisker (c) plots of the di-OVs binding energy as a function of the distance between two oxygen vacancies; Histogram (b) and box-and-whisker plot (d) of the di-OV binding energy. The average and the median energies are −0.08 and −0.05 eV, respectively, confirming weak interaction between the OVs.

TABLE I. Energy barriers and energy of final configuration (reported in parenthesis) measured with respect to the energy of initial configuration for the migration of OV and HO in a-HfO_2. OV wH means OV migration in the presence of HO defect. The three reactions of Path B are reported in Fig. 6. Energies are in eV.

Migration	Path A	Path B	Path C	Path D
OV	0.60 (-0.05)	2.30 (0.24)	2.64 (-0.02)	2.05 (-0.43)
OV wH	0.72 (0.05)	2.20 (0.25)	2.19 (-0.19)	1.83 (-0.65)
H to OV	0.53 (0.08)	0.42 (-0.02)	1.08 (0.66)	0.90 (0.66)

Ref. [21]) does not suggest a clear trend of OV clustering in general, but small clusters composed of a few OVs can be possibly formed. Previous works reported also small binding energy of OVs, but with a positive sign: 1) averaged formation energy for the second OV is 0.1 eV less than the formation energy of the first OV in a-HfO_2 [21], and 2) binding energy of $0.1 - 0.2$ eV in m-HfO_2 [18].

C. OV and HO Migration

For a-HfO_2 containing OVs and hydrogen atoms, there are many possible migration processes. Here, we considered four of them as listed below.

$$OV(r) \rightarrow OV(r') \quad (4)$$
$$OV(r) + HO(r'') \rightarrow OV(r') + HO(r'') \quad (5)$$
$$OV(r) + HO(r') \rightarrow HO(r) + VO(r') \quad (6)$$
$$OV(r) + OH(r') \rightarrow HO(r) \quad (7)$$

The first process is simply the OV migration; while the second one is the OV migration in the presence of an HO defect. The third process is the migration of a hydrogen atom in the HO defect to an OV, hence the HO and OV defects switch positions. The fourth process is the migration of a hydrogen atom in the OH (hydroxyl) defect to OV, which makes a HO defect. According to *ab initio* calculation, the OH defect is unstable with the presence of a neighboring OV defect, meaning that the hydrogen atom in OH would diffuse to the OV defect without an energy barrier. Therefore, we computed energy barriers only for the first three processes. Four migration pathways, labeled from A to D, are obtained using climbing image NEB with 7 images for each process. The four paths are starting from the same initial position r of the labeled oxygen atom in Fig. 1a. For each path, we considered migration of OV, unperturbed and in the close presence of a hydrogen atom(Figs. 6a and 6b), and migration of hydrogen atom towards OV (Fig. 6c). The energy along each pathway is shown in Fig. 5, and barriers are reported in Table. I

The migration barrier of OV ranges from 2 to 2.6 eV for the three paths (B,C and D), which is in line with neutral OV migration in m-HfO_2 [17]. In contrast, an exceptionally low energy barrier of 0.6 eV is observed (path A). The fact of the low energy barrier points out that the local OV transfer is likely in amorphous HfO_2. A long-range OV migration requires consecutive low energy barriers, which could not be concluded from this study.

The nearby OH defect does not perturb much the OV migration path (see Fig. 6). The energy barrier is changed only by about 0.1-0.5 eV among the four simulated pathways. These observations suggest the presence of HO has a limited impact on the OV migration. However, if an HO defect is close to OV, the atomic hydrogen can migrate from the HO to the OV. In the end, the HO and OV switch position (the third reaction in the list). This switching process between HO and OV is characterized by a low energy barrier, barely 0.5 eV in general, i.e. 0.53 eV and 0.42 eV in paths A and B. Therefore, global migration of HO is possible, if the concentration of OV is high. However, due to the energy difference between initial and final configurations, a high energy barrier like 1 eV can exist for one direction, but a shallow barrier is expected for the reverse direction, as shown by paths C and D in Table. I.

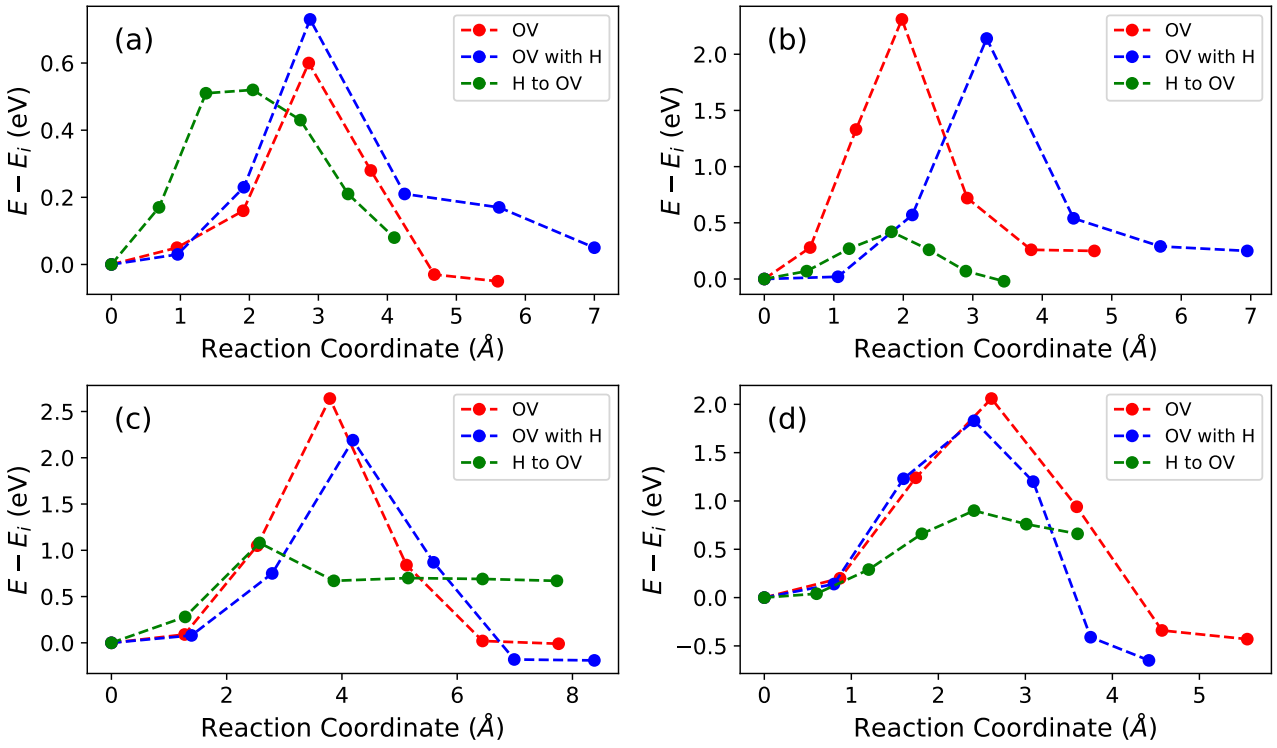

FIG. 5. Panels a, b, c, and d illustrating the evolution of energy along four migration paths, which starts from same position r indicated by the oxygen atom in Fig. 1a. For each path, three types of processes are considered: 1) simple OV migration (red); 2) OV migration in the presence of a nearby OH defect (blue); 3) migration of hydrogen atom in OH defect to OV (green). The trajectories corresponding to the migration path B are shown in Fig. 6.

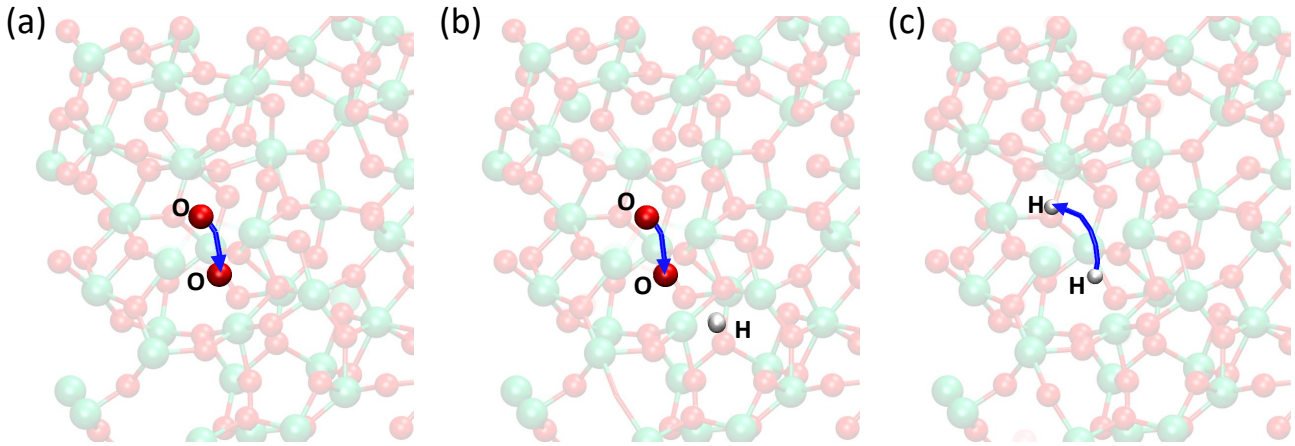

FIG. 6. Migration path B: a) simply OV migration; b) OV migration with the nearby OH defect; c) migration of hydrogen atom in OH defect to OV. Both the initial and final positions of the migrated atom are plotted and The migration path is represented by the blue band. Hafnium, oxygen, and hydrogen atoms are represented by green, red, and white balls.

IV. CONCLUSION

We investigate oxygen vacancy and hydrogen in an a-HfO_2 using DFT *ab initio* methods. The mean formation energy of OV is 6.17 eV with an asymmetric distribution. The tail towards the low energy side is caused by repulsive interaction between the neighboring oxygen atoms, suggesting the presence of "weak spots" in a-HfO_2 based devices. Formation of OVs requires less energy if an over-coordinated oxygen atom is removed from the system.

The binding energy between OVs is weak, with an averaged value of −0.08 eV, not suggesting a global tendency for OVs clustering. However, small clusters of OVs can be formed, as binding energy spans from negative to positive values. Migration of neutral OV in a-HfO_2 is similar to that in m-HfO_2, with a barrier of about 2.4 eV, and is accompanied by possible low-barrier local migrations. The migration process of the OVs remains mostly the same in the presence of hydrogen atoms. However, the hydrogen atom migration is assisted only when an OV is located nearby. This migration process is characterized by a low barrier of 0.5 eV.

ACKNOWLEDGMENTS

This project has received funding from the European Union's Horizon 2020 research and innovation programme under grant agreement No. 871813 MUNDFAB. Calculations were performed on computational resources provided by GENCI–IDRIS (Grant 2021-A0110912036 and Grant 2022-A0130912036).

[1] S. Guha and V. Narayanan, Oxygen vacancies in high dielectric constant oxide-semiconductor films, Physical Review Letters **98**, 196101 (2007).
[2] J. Robertson, High K dielectrics for future CMOS devices, ECS Transactions **19**, 579 (2009).
[3] M. P. Mueller and R. A. De Souza, SIMS study of oxygen diffusion in monoclinic HfO_2, Applied Physics Letters **112**, 051908 (2018).
[4] F. Pan, S. Gao, C. Chen, C. Song, and F. Zeng, Recent progress in resistive random access memories: Materials, switching mechanisms, and performance, Materials Science and Engineering R: Reports **83**, 1–59 (2014).
[5] A. K. Singh, S. Blonkowski, and M. Kogelschatz, Resistive switching study in HfO_2 based resistive memories by conductive atomic force microscopy in vacuum, Journal of Applied Physics **124**, 014501 (2018).
[6] V. Antad, P. A. Shaikh, A. Biswas, S. S. Rajput, S. Deo, M. V. Shelke, S. Patil, and S. Ogale, Resistive switching in $HfO_{2-x}/La_{0.67}Sr_{0.33}MnO_3$ heterostructures: An intriguing case of low H-field susceptibility of an E-field controlled active interface, ACS Applied Materials & Interfaces **13**, 54133–54142 (2021).
[7] J. Strand, M. Kaviani, D. Gao, A.-M. El-Sayed, V. V. Afanas'ev, and A. L. Shluger, Intrinsic charge trapping in amorphous oxide films: status and challenges, Journal of Physics: Condensed Matter **30**, 233001 (2018).
[8] Y. Zhang, G.-Q. Mao, X. Zhao, Y. Li, M. Zhang, Z. Wu, W. Wu, H. Sun, Y. Guo, L. Wang, X. Zhang, Q. Liu, H. Lv, K.-H. Xue, G. Xu, X. Miao, S. Long, and M. Liu, Evolution of the conductive filament system in HfO_2-based memristors observed by direct atomic-scale imaging, Nature Communications **12**, 7232 (2021).
[9] C. N. Singh, B. A. Crafton, M. P. West, A. S. Weidenbach, K. T. Butler, A. H. MacDonald, A. Raychowdury, E. M. Vogel, W. A. Doolittle, L. Piper, and W.-C. Lee, Quantum statistical transport phenomena in memristive computing architectures, Physical Review Applied **15**, 054030 (2021).
[10] K. Xiong, J. Robertson, M. C. Gibson, and S. J. Clark, Defect energy levels in HfO_2 high-dielectric-constant gate oxide, Applied Physics Letters **87**, 183505 (2005).
[11] C. Kaneta and T. Yamasaki, Oxygen-related defects in amorphous HfO_2 gate dielectrics, Microelectronic Engineering INFOS 2007, **84**, 2370–2373 (2007).
[12] S. Zafar, H. Jagannathan, L. F. Edge, and D. Gupta, Measurement of oxygen diffusion in nanometer scale HfO_2 gate dielectric films, Applied Physics Letters **98**, 152903 (2011).
[13] M. Schie, M. P. Müller, M. Salinga, R. Waser, and R. A. De Souza, Ion migration in crystalline and amorphous HfO_x, The Journal of Chemical Physics **146**, 094508 (2017).
[14] S. Swathi and S. Angappane, Enhanced resistive switching performance of hafnium oxide-based devices: Effects of growth and annealing temperatures, Journal of Alloys and Compounds **913**, 165251 (2022).
[15] H. Sim and H. Hwang, Effect of deuterium postmetal annealing on the reliability characteristics of an atomic-layer-deposited HfO_2/SiO_2 stack gate dielectrics, Applied Physics Letters **81**, 4038–4039 (2002).
[16] D. Duncan, B. Magyari-Köpe, and Y. Nishi, Hydrogen doping in HfO_2 resistance change random access memory, Applied Physics Letters **108**, 043501 (2016).
[17] N. Capron, P. Broqvist, and A. Pasquarello, Migration of oxygen vacancy in HfO_2 and across the HfO_2SiO_2 interface: A first-principles investigation, Applied Physics Letters **91**, 192905 (2007).
[18] S. R. Bradley, G. Bersuker, and A. L. Shluger, Modelling of oxygen vacancy aggregates in monoclinic HfO_2: can they contribute to conductive filament formation?, Journal of Physics: Condensed Matter **27**, 415401 (2015).
[19] J. W. Strand, J. Cottom, L. Larcher, and A. L. Shluger, Effect of electric field on defect generation and migration in hfo_2, Physical Review B **102**, 014106 (2020).
[20] M. Kaviani, V. V. Afanas'ev, and A. L. Shluger, Interactions of hydrogen with amorphous hafnium oxide, Physical Review B **95**, 075117 (2017).
[21] D. Z. Gao, J. Strand, M. S. Munde, and A. L. Shluger, Mechanisms of oxygen vacancy aggregation in SiO_2 and HfO_2, Frontiers in Physics **7** (2019).
[22] G. Broglia, G. Ori, L. Larcher, and M. Montorsi, Molecular dynamics simulation of amorphous $HfO_2$for resistive RAM applications, Modelling and Simulation in Materials Science and Engineering **22**, 065006 (2014).
[23] G. Kresse and D. Joubert, From ultrasoft pseudopotentials to the projector augmented-wave method, Physical Review B **59**, 1758–1775 (1999).
[24] J. P. Perdew, K. Burke, and M. Ernzerhof, Generalized gradient approximation made simple, Physical Review Letters **77**, 3865–3868 (1996).
[25] G. Henkelman, B. P. Uberuaga, and H. Jónsson, A climbing image nudged elastic band method for finding saddle

points and minimum energy paths, The Journal of Chemical Physics **113**, 9901–9904 (2000).

[26] D. Sheppard, P. Xiao, W. Chemelewski, D. D. Johnson, and G. Henkelman, A generalized solid-state nudged elastic band method, The Journal of Chemical Physics **136**, 074103 (2012).

[27] J. Zhang, A. R. Oganov, X. Li, K.-H. Xue, Z. Wang, and H. Dong, Pressure-induced novel compounds in the Hf-O system from first-principles calculations, Physical Review B **92**, 184104 (2015).

[28] W. Tang, E. Sanville, and G. Henkelman, A grid-based Bader analysis algorithm without lattice bias, Journal of Physics: Condensed Matter **21**, 084204 (2009).

[29] T.-J. Chen and C.-L. Kuo, First principles study of the structural, electronic, and dielectric properties of amorphous HfO_2, Journal of Applied Physics **110**, 064105 (2011).